

# Excessive activation of IL-33/ST2 in cancer-associated fibroblasts promotes invasion and metastasis in ovarian cancer

CAIXIA FENG<sup>1</sup>, LI KOU<sup>2</sup>, PANYUE YIN<sup>2</sup> and YUAN JING<sup>2</sup>

<sup>1</sup>Department of Obstetrics and Gynecology, Yulin First Hospital, Yulin, Shaanxi 719000;

<sup>2</sup>Department of Gynecology, Baoji People's Hospital, Baoji, Shaanxi 721000, P.R. China

Received April 8, 2020; Accepted December 1, 2020

DOI: 10.3892/ol.2022.13278

**Abstract.** Ovarian cancer is highly prevalent and has high mortality rates due to metastasis and relapse. The cross communication between cancer-associated fibroblasts (CAFs) and cancer-associated macrophages (CAMs) in the ovarian tumor microenvironment leads to cancer cell invasion and metastasis. However, the role of overproduction of IL-33/ST2 in the CAFs of ovarian cancer is still unclear. The expression of IL-33, ST2, apoptosis-related proteins and epithelial-mesenchymal transition (EMT) markers was measured by western blotting. Primary normal fibroblasts and CAFs from ovarian cancerous tissue were isolated and cultured *in vitro*, and the medium was used to stimulate blood-derived monocytes. Flow cytometry analysis was used to detect the frequency of M2-like macrophages in blood-derived monocytes from patients with ovarian cancer. Cell invasion were evaluated using Transwell assays. A xenograft model was used to study tumor growth in ST2-knockout and wild-type NOD-SCID mice. The results demonstrated higher expression of IL-33 and ST2 in carcinoma tissues compared with in para-carcinoma tissues, and there was a survival improvement associated with elevated IL-33. IL-33 and culture supernatants from CAFs, rather than normal ovarian fibroblasts, led to a higher expression of M2 macrophage marker genes in human blood-derived monocytes. Invasion and migration were aggravated in COC1 cells co-cultured with CAF-induced CAMs, and the EMT marker genes were upregulated. It was reported that EMT marker genes were downregulated and tumor volumes were significantly reduced in ST2-deficient mice. Overall, the IL-33/ST2 axis in ovarian cancer might integrate IL-33-expressing CAFs with M2 type-like CAMs, which aggravated invasion and metastasis by promoting EMT.

## Introduction

Ovarian carcinoma is a major gynecological malignant tumor with high incidence and mortality (1). In China, ovarian carcinoma has increased significantly by nearly 30% in recent years (1). Although the mortality of ovarian cancer generally decreases with early diagnosis and treatment, patients with advanced or late stage of ovarian squamous cell carcinoma (OSCC) still have a poor prognosis, with a 5-year survival rate of below 20% in China (1,2).

Epithelial ovarian cancer is the leading pathological type of ovarian malignant tumors and accounts for nearly 50% in all types of ovarian malignant tumor worldwide (3,4). The tumor microenvironment plays an important role in invasion and metastasis, and is composed of cancer-associated fibroblasts (CAFs) and other types of stromal cells, including endothelial cells and inflammatory cells (5). CAFs can regulate tumor biological processes and contribute to cancer progression by various mechanisms, such as affecting extracellular matrix (ECM) remodeling (6). CAFs also secrete inflammatory cytokines, which could play an important role in the regulation of immune cells (6). TGF- $\beta$  is a cytokine that is mainly secreted by CAFs, which can promote the epithelial-mesenchymal transition (EMT), contributing to the invasion and metastasis in colorectal and breast cancer (7). In addition, CAFs play a vital role in ECM remodeling through the regulation of production and degradation of metalloproteinases via Rho/Rho-associated protein kinase signaling (8). The physical remodeling of ECM enhances tumor growth and facilitates metastatic invasion in various cancer types, such as breast cancer (9), pancreatic cancer (10), colorectal cancer (11). In addition, CAFs also can synthesize soluble inflammatory tumor-promoting factors involved in cancerous biological processes, such as stromal cell-derived factor 1, which enhances invasiveness via activation of integrin  $\beta$ 1-related signaling pathways (9). In addition, the co-culture of CAFs with melanoma cells results in the production of various pro-inflammatory cytokines, such as interleukin (IL)-6, IL-8 and IL-1 $\beta$  and concurrently represses the expression of inflammatory mediators that inhibit the invasiveness of cancer cells (12). These results indicated that CAFs serve a key role in the regulation of immune responses by secreting several inflammatory mediators (12-14).

---

*Correspondence to:* Dr Yuan Jing, Department of Gynecology, Baoji People's Hospital, 24 Xinhua Lane, Baoji, Shaanxi 721000, P.R. China  
E-mail: jingy0201@163.com

**Key words:** IL-33, cancer-associated fibroblast, metastasis, ovarian cancer, M2 macrophage

Cancer-associated fibroblasts can also secrete exosomes that transport mediators of cell-cell communication in a paracrine manner, including non-coding RNA molecules or some inflammatory mediators, such as IL-33, IL-1 $\beta$  and tumor necrosis factor (TNF)- $\alpha$  (15). A previous report showed that the components in exosomes produced by CAFs could promote breast cancer cell motility and metastasis via activation of Wnt-planar cell polarity (Wnt-PCP) cell signaling (16). Exosome-stimulated breast cancer cells display excessive activation of Wnt-planar cell polarity signaling (15). In breast cancer mouse models, administration of breast cancer cells (BCCs) combined with fibroblasts promotes metastasis dependent on cell-cell communication mediators contained in exosomes, Cd81 and Wnt-PCP signaling in BCCs (15,16).

The present study aimed to demonstrate the role of IL-33 transported by exosomes secreted by CAFs in ovarian epithelial carcinoma by regulation of the differentiation and function of cancer-associated macrophages (CAMs).

## Materials and methods

**Animals.** Wild-type (WT) and ST2-deficient female nude BALB/c mice were purchased from the Experimental Animal Center of Nanjing University. The protocols for animal experiments were approved by the Baoji People's Hospital Ethics Committee on the Use of Live Animals in Teaching and Research (Baoji, China). A total of 30 female mice (12 weeks old) with a weight of  $\sim 30$  g were housed under 12 h of light and 12 h dark cycle with free access to food and water at the Laboratory Animal Unit.

**Cell culture.** The human ovarian cancer cell line COC1 was purchased from the American Type Culture Collection. COC1 cells were cultured in DMEM with 1,000 mg/l D-Glucose (Stemcell Technologies, Inc.) supplemented with 10% FBS (Thermo Fisher Scientific, Inc.) and 100 U/ml of penicillin/streptomycin (Thermo Fisher Scientific, Inc.) in a humidified incubator. Primary normal ovarian fibroblasts (NOFs) and CAFs were isolated from human benign ovarian biopsies from five patients with ovarian epithelial cancer and five patients with benign ovarian cysts in the Yulin First Hospital (Yulin, China) from February 2018 to September 2019. The mean  $\pm$  SD age of these subjects was 56.5 $\pm$ 8.2 years. Verbal informed consent was provided by all patients. Briefly, the stroma was separated from the ovarian epithelial tissues after incubation overnight at 4°C in HEPES buffer with 500  $\mu$ g/ml thermolysin (Sigma-Aldrich; Merck KGaA). The fibroblasts were enzymatically dissociated from the ECM by treating the stroma with 0.125 U/ml collagenase H (Roche Diagnostics) for 30 min at 37°C under gentle agitation. Then, fibroblasts were cultured in DMEM supplemented with 10% FBS (Invitrogen; Thermo Fisher Scientific, Inc.) and antibiotics (100 U/ml penicillin and 25  $\mu$ g/ml gentamicin; Sigma-Aldrich; Merck KGaA). All cells were cultured for fewer than three passages after purchasing or receiving them for all the experiments and tested for mycoplasma contamination by microscopic examination. The CAFs and NOFs were centrifuged at 1,000 x g at room temperature and the supernatants were collected and stored at -80°C until further experiments. The venous blood-derived monocytes from the aforementioned patients

mentioned were also isolated. The CD14<sup>high</sup> or CD16<sup>high</sup> blood-derived monocytes were sorted by flow cytometry sorting technology from peripheral blood mononuclear cells (PBMCs) isolated by Ficoll centrifugation at 1,000 x g at 25°C according to the markers of CD14 and CD16. Blood monocyte cells were cultured in RPMI-1640 medium supplemented with 10% FBS (Thermo Fisher Scientific, Inc.) and 100 U/ml of penicillin/streptomycin (Thermo Fisher Scientific, Inc.) in a humidified incubator.

**Isolation of exosomes derived from NOFs and CAFs.** CAFs and NOFs cellular supernatant was treated with the FBS Exosome Depletion kit (Norgen Biotek Corp.) to remove any residual bovine exosomes in FBS, according to the manufacturer's instructions. CAFs and NOFs isolated from normal ovarian tissues and cancerous tissues were cultured in DMEM containing 10% exosome-depleted FBS for 48 h. Then, the conditioned medium was centrifuged at 2,000 x g for 30 min to remove cells and debris, and the supernatant was mixed with 0.5 ml volume of the Total Exosome Isolation Reagent (Invitrogen; Thermo Fisher Scientific, Inc.). Samples were mixed by vortexing and incubated at 4°C overnight. Then, they were centrifuged at 10,000 x g for 60 min at 4°C. Exosomes, contained in the pellet, were resuspended in PBS. The protein concentration was measured using a BCA kit (Pierce; Thermo Fisher Scientific, Inc.). Transmission electron microscopy (Hitachi HT7700; Hitachi Ltd.) was used for the visualization of extracellular vesicles (exosomes). Briefly, the isolated exosomes were fixed with 2% paraformaldehyde for 15 min at 37°C and spotted onto a glow-discharged copper grid on filter paper. Then, the copper grids were dried for 15 min at room temperature to remove the excessive liquid. The samples were stained by 2% phosphotungstic acid (PTA) for 5 min at room temperature. Subsequently, the samples were examined at 100 keV. The mean diameter and concentration per milliliter of exosomes were calculated by the qNano (Izon Science Ltd.).

**Pathological examination by immunofluorescence staining.** The ovarian epithelial cancerous tissues were fixed with 4% (v/v) paraformaldehyde for 24 h at 25°C and cut into 5- $\mu$ m slices. For immunocytochemistry, permeabilization was performed using 0.25% (v/v) Triton X-100/PBS (Sigma-Aldrich; Merck KGaA) for 30 min followed by blocking using 5% BSA in PBS for 30 min at 25°C. Incubation with primary antibodies against  $\alpha$ -SMA (1:1,000; cat. no. ab7817; Abcam), IL-33 (1:1,000; cat. no. ab187060; Abcam), PAX8 (1:1,000; cat. no. 406421; BioLegend, Inc.) and CD45 (1:2,000; cat. no. ab40763; Abcam) was performed at room temperature for 1 h in PBS containing 5% BSA. The tissue slices were rinsed in PBS before incubation with anti-rabbit Alexa Fluor 488-conjugated secondary antibody and anti-mouse Alexa Fluor 647-conjugated secondary antibody (both 1:1,000; cat. nos. R37116 and A32731; Invitrogen; Thermo Fisher Scientific, Inc.) for 1 h. Nucleus staining was performed with DAPI for 5 min at 25°C (Vector Laboratories, Inc.; Maravai LifeSciences). The co-localization of IL-33-positive cells with other markers staining positive cells was visualized using a fluorescence microscope (Olympus Corporation).

**Western blotting.** Total protein of blood-derived monocytes and ovarian cancerous tissues were extracted by RIPA lysis and

Table I. Primer sequences used for reverse transcription-quantitative PCR.

Gene	Forward (5'-3')	Reverse (5'-3')
CD209	GATGCAGGGTTGGACAA	GCCATCCATTGGACCCATC
MRC1	ATGCGATGCCCTACAGC	TCGACTACGTTGGACCAA
SLC40A1	CTGACTGTTTCACGGGAT	CTGACTGCATTCCAGCCT
FOLR2	TCAGTCAGACCTTACCAT	TCGAGGCTGCTTGCCTC
GAPDH	CAGGCCTGCAGCCTGCT	TGTCCAACCTTAGCCACCC

MRC1, mannose receptor C-type 1; SLC40A1, solute carrier family 40 member 1; FOLR2, folate receptor  $\beta$ .

extraction buffer (Thermo Fisher Scientific, Inc.) and T-PER™ tissue protein extraction reagent (cat. no. 78510; Thermo Fisher Scientific, Inc.). Equal amounts of protein (10  $\mu$ g/lane) were loaded onto 12% polyacrylamide gels, resolved by SDS-PAGE and transferred to polyvinylidene difluoride membranes. The membranes were blocked for 30 min with 5% non-fat milk and 0.05% Tween-20 in PBS at 4°C. The membranes were incubated with primary antibodies overnight at 4°C followed by 45 min at room temperature with HRP-conjugated secondary antibodies (Jackson ImmunoResearch Laboratories, Inc.). Protein expression was detected using Amersham ECL Western Blotting Detection reagent (GE Healthcare). Bands were visualized using a Fusion Fx7 imager (Vilber Lourmat) and analyzed using ImageJ software v.6.0 (National Institutes of Health). The following antibodies were used: TGF- $\beta$  (1:1,000; cat. no. 846802; BioLegend, Inc.), NF- $\kappa$ B p65 (1:2,000; cat. no. ab207297; Abcam), I $\kappa$ B (1:1,000; cat. no. AI096-1; BioLegend, Inc.), I $\kappa$ K (1:1,000; cat. no. ab32518; Abcam), cleaved caspase-3 (1:1,000; cat. no. 25546-1-AP; ProteinTech, Inc.), cleaved caspase-8 (1:1,000; cat. no. ab32397; Abcam),  $\alpha$ -SMA (1:2,000; cat. no. ab5931; Abcam), vimentin (1:1,000; cat. no. ab92547; Abcam), GAPDH (1:5,000; cat. no. ab8245; Abcam), ZEB1 (1:1,000; cat. no. ab203829; Abcam), Snail (1:1,000; cat. no. ab216347; Abcam), ST2 (1:1,000; cat. no. ab194113; Abcam), IL-33 (1:1,000; cat. no. H00090865-B01; Novus Biologicals), p-Smad2 (1:100; cat. no. ab280888; Abcam), p-Smad3 (1:1,000; cat. no. ab52903; Abcam) and tubulin (1:1,000; cat. no. NA100-1639; Novus Biologicals, Ltd.).

**Reverse transcription-quantitative PCR.** Total RNA of ovarian cancerous tissues was extracted using TRIzol® reagent according to the manufacturer's instructions (Invitrogen; Thermo Fisher Scientific, Inc.). RNA concentration and purity were confirmed using a Nanodrop 2000 (Thermo Fisher Scientific, Inc.). Samples with a relative absorbance ratio of 260/280 between 1.8 and 2.0 were used. All RNA samples were reverse-transcribed using the High-capacity cDNA reverse transcription kit (cat. no. 4368813; Applied Biosystems; Thermo Fisher Scientific, Inc.) according to manufacturer's protocol. Quantification of specific mRNAs was performed using an ABI PRISM 7300 Sequence Detection system (Applied Biosystems; Thermo Fisher Scientific, Inc.) with the SYBR Green Real-time PCR kit (Takara Bio, Inc.). The thermocycling conditions used were as follows: 35 cycles of 94°C for 10 min, 55°C for 1 min and 70°C for 10 min. The primer sequences used in the study are shown in Table I. Relative

mRNA amounts were normalized to GAPDH and calculated using the standard curve method (17). In brief, the pre-PCR product of each gene was used as the standard. The standard curve was established with a 10-fold serial dilution of the product and was included in all PCR runs. The ratio of target housekeeping gene was used to determine the expression level of each gene. A control consisting of ddH<sub>2</sub>O was negative in all runs.

**ELISA.** The cell supernatant was collected, and the concentration of TGF- $\beta$  and IL-10 were measured using a commercially available ELISA kit (cat. no. D1000B; R&D Systems, Inc.) according to the protocol described by the manufacturer.

**Flow cytometry.** After stimulation, PBMCs and blood-derived monocytes were cultured in RPMI-1640 medium with 10% FBS and resuspended at a density of 0.5x10<sup>5</sup> cells per ml. The cells were then stained with directly conjugated antibodies for 30 min at 4°C in flow tubes, and then fixed with PBS containing 4% paraformaldehyde. The antibodies used for flow cytometry included anti-human CD16-APC (cat. no. 561304), anti-human CD14-PeCy7 (cat. no. 557154), anti-human CD206-APC-Cy7 (cat. no. 551136) and anti-human 163-Alexa Fluor 488 (cat. no. 560459) (all BD Biosciences). For the flow cytometry analysis, the cells were collected according to the multi-color flow cytometer (BD Biosciences), and the FACS data were analyzed using FlowJo 10.0 software (BD Biosciences). For monocyte sorting, CD14<sup>high</sup> or CD16<sup>high</sup> monocytes were isolated from PBMCs according to standard protocols.

**Transwell assay.** Cells were suspended in serum-free medium at a density of 1.0x10<sup>5</sup>/ml. Transwell chambers with or without Matrigel pre-coating were inserted into 24-well plates containing 200  $\mu$ l of the cell suspension in the apical chamber and 500  $\mu$ l of medium with 10% FBS in the basolateral chamber at 37°C. At 48 h, the chambers were removed and the penetrating cells were fixed with 5% paraformaldehyde for 20 min 25°C and dyed with 0.1% crystal violet for 20 min at 25°C. Images of penetrating cells in four randomly selected fields of each sample were captured for counting using a light microscope (magnification, x20; Olympus Corporation). Transwell chambers for the invasion assay were pre-coated with Matrigel at room temperature for 30 min.

**Cell viability analysis.** COC1 cells were maintained in RPMI-1640 medium (Sigma-Aldrich; Merck KGaA),

supplemented with 10% FBS at 37°C in a humidified atmosphere with 5% CO<sub>2</sub>. Different concentrations of cisplatin (at concentrations of 2, 4, 8 and 16 µg/ml) were used to treat the cells. After 48 h incubation at 37°C, cells were subjected to MTT reagent dissolved in DMSO for 4 h, and the absorbance at 570 nm was recorded using a Spectra Max i3 microplate reader (Molecular Devices, LLC).

**Xenograft models in mice.** Female 4-week old BALB/c mice (weight, ~15 g) with or without ST2-deficiency were bred and purchased from the Model Animal Research Center of Nanjing University. The mice were housed with a 12 h of light and 12 h dark cycle with free access to food and water in a pathogen-free environment. A xenograft humanized ovarian carcinoma mouse model was established by injecting 1x10<sup>7</sup> COC1 cells subcutaneously in the flank region of each female nude BALB/c mice with or without ST2-deficiency. After 4 days, the mice were euthanized by intraperitoneal injection of phenobarbital at a dose of 0.1 mg/g of body weight. The loss of breath (disappearance of thorax movement) and adiphoria to clamping of the toes were used to confirm death. The engrafting tumors were harvested, weighed and then used for protein isolation and immunoblot assays.

**Immunohistochemical staining.** A total of 156 patients with ovarian cancer (median age 61 years; age range, 35–69 years) were included in the present retrospective study. The carcinoma tissues from these patients were fixed in 5% formalin at room temperature for 30 min and then embedded in paraffin blocks after surgical resection. Before immunohistochemical staining, antigens were retrieved according to the thermal remediation method (18), and the slides were incubated at 25°C with 3% goat serum (cat. no. C0265; Beyotime Institute of Biotechnology) for 30 min. The paraffin block was cut into 5-µm sections and then incubated with primary antibodies against rat anti-human IL-33 (cat. no. ab187060) and ST2 (cat. no. ab194113) (both Abcam) in 5% rabbit serum (cat. no. BMS0090; Abbkine Scientific Co., Ltd.) overnight at 4°C followed by washing and incubation with avidin-linked biotin complex rabbit anti-rat Ig (cat. no. 5597; Cell Signaling Technology Inc.). The signals were detected using a DAB substrate and hematoxylin was used for counterstaining at room temperature for 5 min, respectively. The slides were dehydrated by ethanol, cover slips were added, and they were observed under a light microscope (magnification, x20) (Zeiss GmbH). A negative control in the absence of primary antibodies and incubated with isotype-matched immunoglobulins was also used for immunostaining. All captured images were analyzed by ImageJ to quantify the expression levels of IL-33 and ST2, according to the ratio of fluorescent intensity of primary antibody-stained sections to the negative control. The mean expression level was used to divide the subjects into two groups.

**Statistical analysis.** All data were presented as mean ± SD. The experiments were repeated 3 times. Unpaired Student's t-tests or Mann-Whitney tests were applied to analyze the difference between two groups. One-way ANOVA was used to analyze the difference among three groups. Survival curves were depicted by Kaplan-Meier methods and the difference

between two groups was analyzed using the log-rank test. P<0.05 was considered to indicate a statistically significant difference. P-values were two-tailed. All statistical tests were performed using SPSS statistical software, version 24.0 (IBM Corp.).

## Results

**A higher expression of IL-33 in cancerous tissues correlates with poor prognosis.** To explore the potential role of the IL-33/ST2 axis in ovarian cancer, the expression levels of IL-33 and ST2 were measured using by immunoblot assays and RT-qPCR. IL-33 and ST2 expression in cancerous tissues was significantly higher compared with para-carcinoma tissues (n=10; both P<0.001; Fig. 1A and B). To investigate whether higher expression of IL-33 and ST2 was associated with prognosis, survival analysis in a prospective cohort was performed, including 156 patients according to the expression levels measured by immunohistochemical staining. It was reported that 67 out of 156 patients with an increased expression of IL-33 had significantly poorer overall survival time (OS) (P=0.010) and progression-free survival time (PFS) (P=0.012) compared with those with a lower expression of IL-33 (Fig. 1C and D). Higher expression levels of ST2 in cancerous tissue were also associated with poor 3-year OS (P<0.001) and PFS (P=0.002) (Fig. 1E and F). To determine the cellular source of IL-33 in the cancerous tissues, double immunohistochemical staining using IL-33 and cellular markers of ovarian epithelial cancer cells, inflammatory cells and cancer-associated fibroblasts, including PAX8, CD45 and α-SMA, was performed. There was prominent co-location of α-SMA with IL-33 and rare IL-33-producing CD45<sup>+</sup> and PAX8<sup>+</sup> cells in cancerous tissues (Fig. 1G). The results suggested that cancer-associated fibroblasts could produce more IL-33 compared with ovarian epithelial cancer cells and CD45<sup>+</sup> inflammatory cells.

**Human recombinant IL-33 and supernatants from cultured primary cancer-associated fibroblasts promote the differentiation of blood-derived monocytes into M2-like macrophages.** Primary CAFs were isolated and cultured from five patients with ovarian cancer recurrence after surgical resection and chemotherapy. Then NOFs were isolated from five patients with benign ovarian tumors. After 7 days, the supernatant of NOFs and CAFs was extracted and used to obtain blood-derived monocytes from the same individuals. Significantly elevated expression of M2 markers was observed, including CD209, mannose receptor C-Type 1 (CD206; MRC1), solute carrier family 40 member 1 (SLC40A1) and folate receptor β (n=5; P<0.05; Fig. 2A) in blood-derived monocytes cultured with supernatant from primary CAFs compared with NOFs. The concentrations of IL-10 and TGF-β were also significantly elevated after stimulation with IL-33 or the supernatant from primary CAFs compared with the NOFs (n=5; P<0.05; Fig. 2B). Blood-derived monocyte cells were harvested after 3 days and flow cytometry analysis was performed to measure the frequency of M2-macrophages. There was a significantly higher frequency of CD163<sup>high</sup>CD209<sup>high</sup> M2-macrophages in the blood-derived monocytes stimulated by human recombinant IL-33 and supernatant of CAFs compared with the control (n=5; P<0.001; Fig. 2C). The expression of proinflammatory

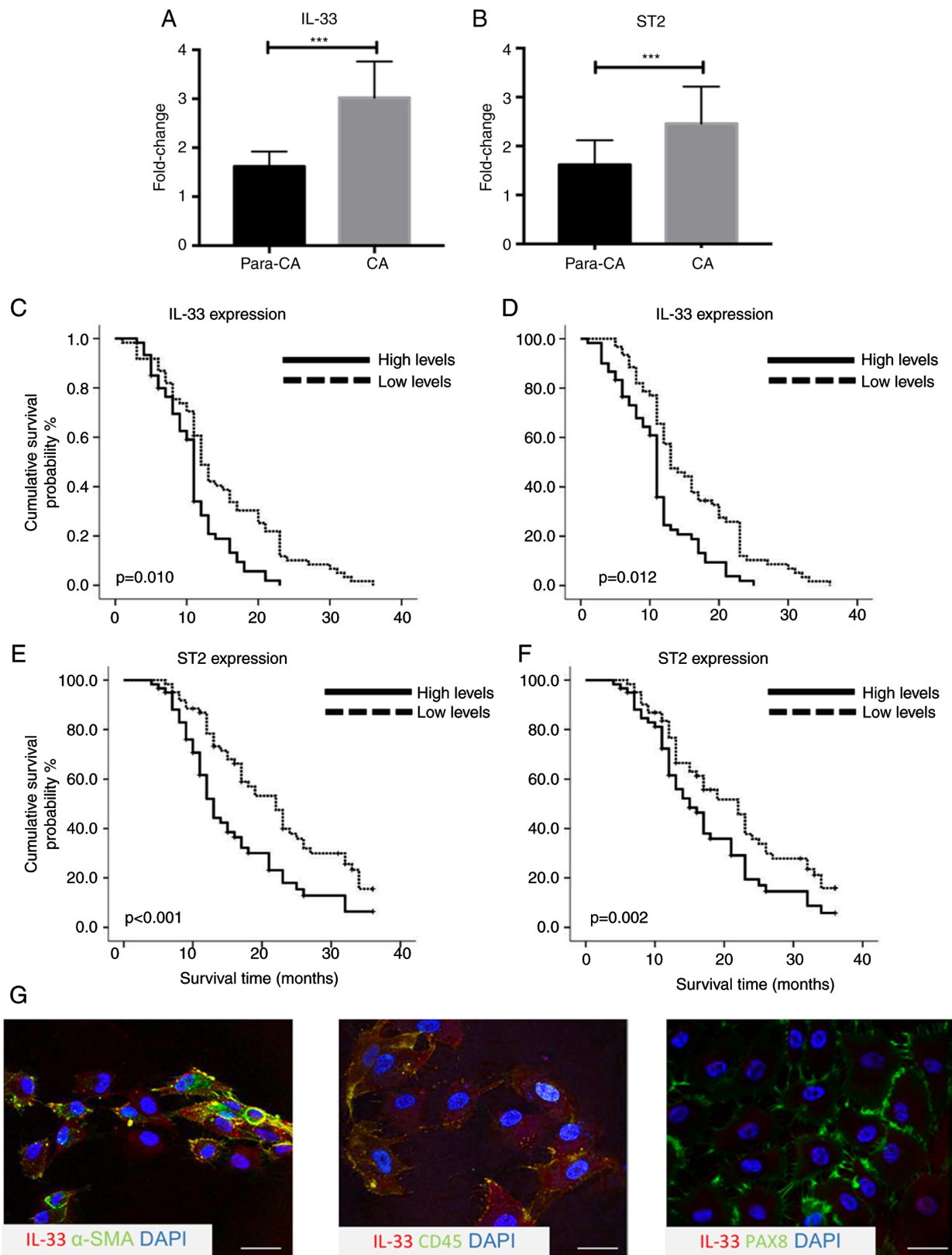


Figure 1. Higher expression of IL-33 in cancerous tissues is associated with improved overall and progression-free survival. Expressions of (A) IL-33 and (B) ST2 in the para-carcinoma and carcinoma tissues from patients with ovarian cancer measured using reverse transcription-quantitative PCR (n=10). Survival analysis of the association between the expression of IL-33 and (C) OS and (D) PFS (n=156), and association between the expression of ST2 and (E) OS and (F) PFS (n=156). (G) Co-localization of IL-33 with  $\alpha$ -SMA but without PAX8 and CD45 detected by immunofluorescence staining. \*\*\* $P<0.001$ . OS, overall survival; PFS, progression-free survival; ST2, interleukin-1 receptor-like 1.

cytokines, including IL-1 $\beta$ , TNF- $\alpha$  and IL-6, were significantly decreased in the blood-derived monocytes cultured by human

recombined IL-33 and the supernatant of CAFs compared with controls (n=5;  $P<0.01$  or  $P<0.05$ ; Fig. 2D). Meanwhile,

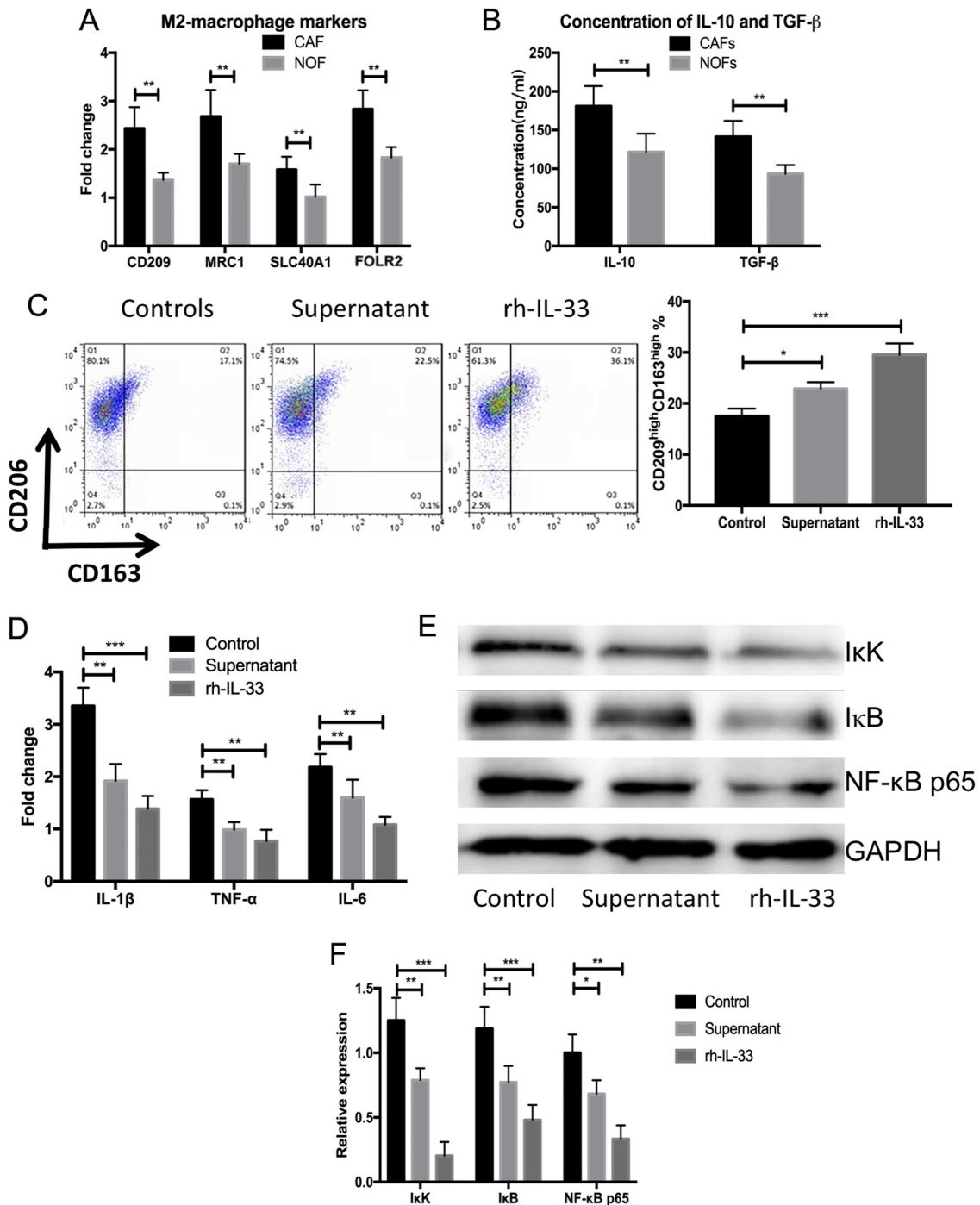


Figure 2. rh-IL-33 and supernatant from cultures primary cancer-associated fibroblasts promote the differentiation of blood-derived monocyte towards M2-like macrophages. (A) Higher expression of M2 markers, including CD209, MRC1, SLC40A1 and FOLR2, in the blood-derived stimulated by supernatant of NOFs and CAFs measured using western blot assays. (B) Higher concentration of IL-10 and TGF-β in the supernatant of NOFs and CAFs after stimulation with IL-33 or the supernatant from primary CAFs. (C) Higher frequency of CD163<sup>high</sup> CD209<sup>high</sup> M2-macrophages in the blood-derived monocytes stimulated with human recombinant IL-33 and supernatant of CAMs. (D) Expression of proinflammatory cytokines including IL-1β, TNF-α and IL-6 in the blood-derived monocytes cultured with human recombinant IL-33 and supernatant of CAMs. (E and F) Expressions of NF-κB signaling-related proteins measured using western blot assays. \*P<0.05, \*\*P<0.01 and \*\*\*P<0.001. SLC40A1, solute carrier family 40 member 1; NOF, normal ovarian fibroblasts; CAF, cancer-associated fibroblasts; rh-IL-33, recombination human interleukin-33; FOLR2, folate receptor β.

NF-κB signaling-related proteins were significantly decreased in the blood-derived monocytes treated with human recombinant IL-33 and the supernatant of CAFs compared with the control (n=5; P<0.001 or P<0.05; Fig. 2E and F). These results demonstrated that IL-33 could lead to the differentiation of M2-like macrophages and the secretion of anti-inflammatory cytokines.

*Increased EMT in ovarian cancerous cells co-cultured with CAF-induced CAMs.* To explore the expression of marker genes associated with EMT in COC1 cells, the levels of vimentin, Snail, α-SMA and ZEB1 were analyzed. Notably, similar expression levels of EMT markers in COC1 cells treated with CAF and NOF medium were observed (n=5; P<0.05; Fig. 3A). The concentrations of IL-10 and TGF-β were similar between

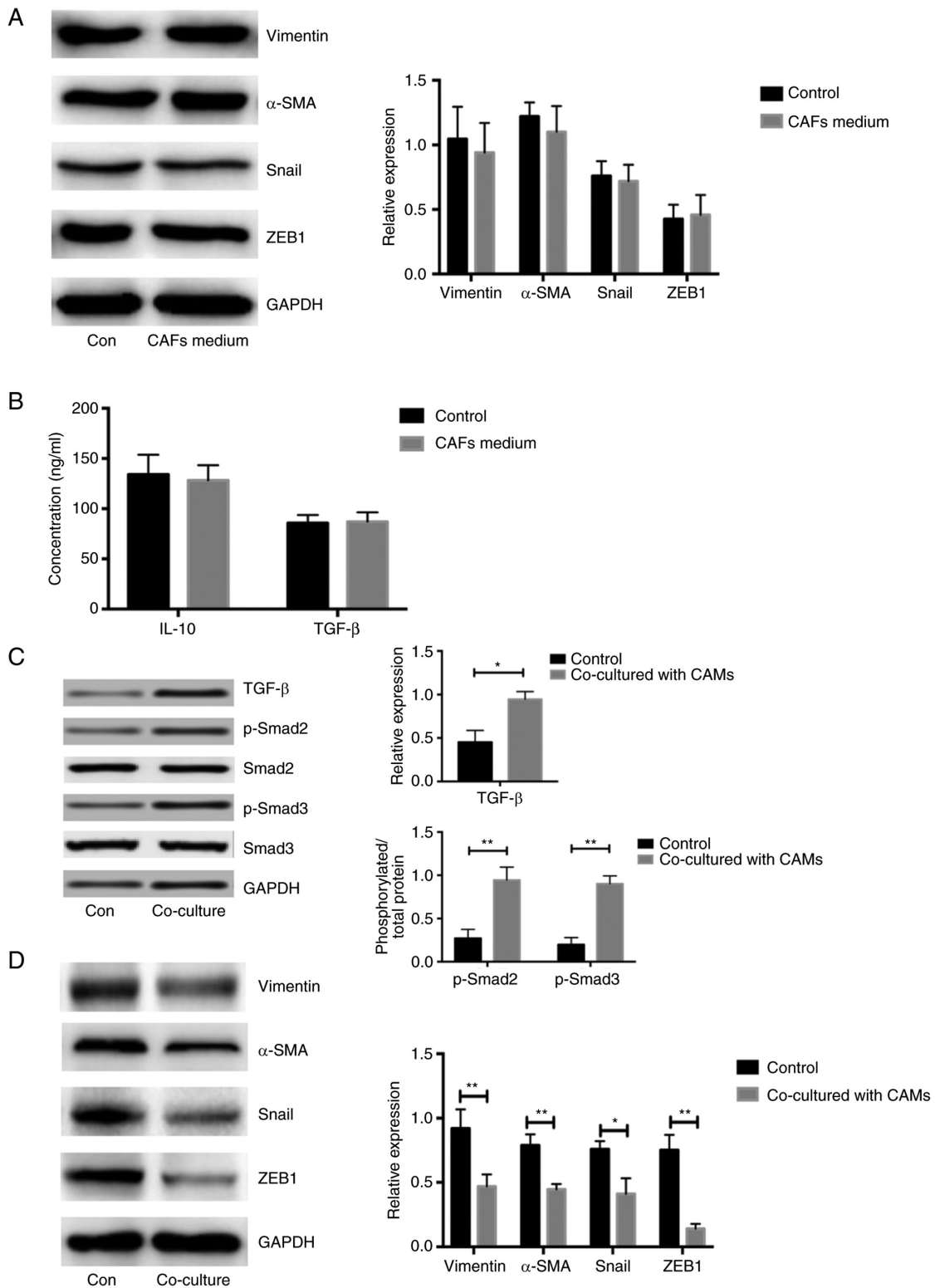


Figure 3. Increased EMT in the ovarian cancerous cells co-cultured by CAF-induced CAMs. (A) Expressions of genes related to EMT in COC1 cells treated with medium from NOFs and CAFs. (B) Concentration of IL-10 and TGF-β measured by ELISA assays in the COC1 cells treated by the mediums from CAFs and NOF, respectively. (C) Expression of TGF-β and phosphorylation of Smad2/3 in the COC1 cells treated with co-cultured with CAF-induced CAMs and controls, respectively. (D) Expression of proteins associated with EMT in the COC1 cells co-cultured with CAF-induced CAMs and controls. \*P<0.05, \*\*P<0.01. NOF, normal ovarian fibroblasts; CAF, cancer-associated fibroblasts; CAM, cancer-associated macrophage; EMT, epithelial-mesenchymal transition.

the media directly derived from CAFs and NOFs, respectively (n=5; P<0.05; Fig. 3B). Due to the increased concentration of TGF-β in the CAMs stimulated with CAF supernatant, the expression of proteins associated with TGF-β/Smad signaling

were measured. The expression of TGF-β and phosphorylation of Smad2/3 was significantly higher in the COC1 cells co-cultured with CAF-induced CAMs compared with that in controls, respectively, (n=5; P<0.05; Fig. 3C). The expression

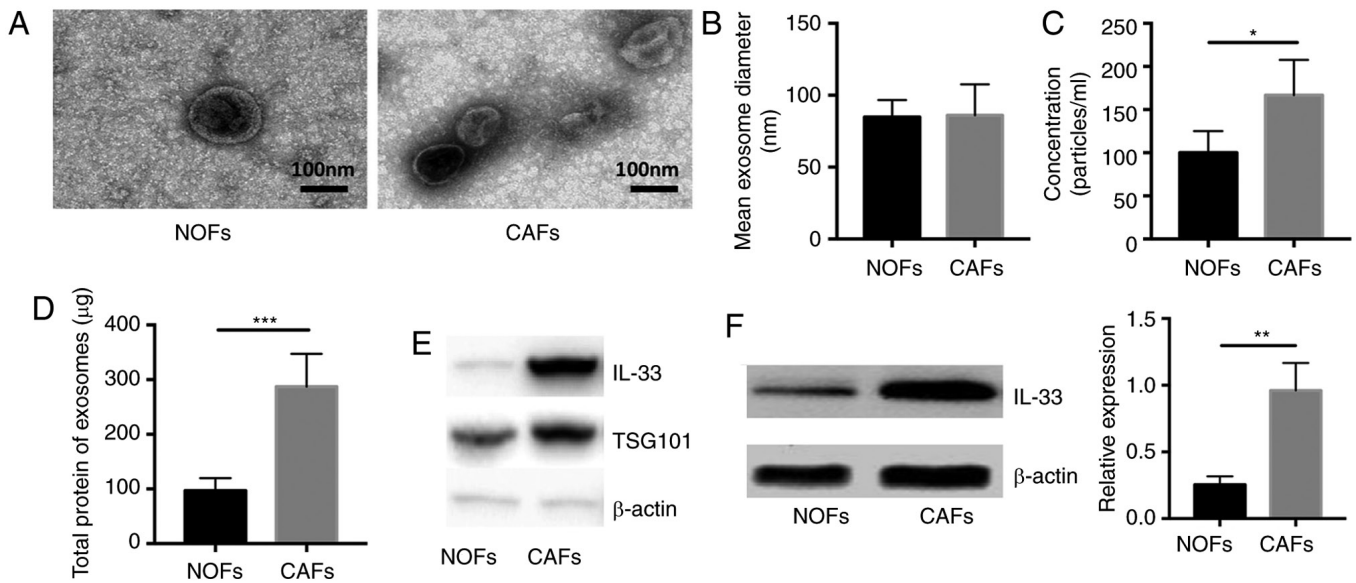


Figure 4. Size, number and expression of IL-33 in the isolated exosomes from NOFs and CAFs. (A) Shapes of extracellular vesicles isolated from NOFs and CAFs by transmission electron microscopy. Scale bar, 100 nm. (B) Size diameter and (C) concentration of extracellular vesicles isolated from NOFs and CAFs. (D) Volume of total protein in the exosomes from supernatant of NOFs and CAFs. (E) Expressions of IL-33, TSG101 and  $\beta$ -actin in exosomes isolated from supernatant NOFs and CAFs. (F) Expression of IL-33 in the NOFs and CAFs. \* $P < 0.05$ , \*\* $P < 0.01$  and \*\*\* $P < 0.001$ . NOF, normal ovarian fibroblasts; CAF, cancer-associated fibroblasts.

of genes associated with the EMT process in COC1 cells co-cultured with CAF-induced CAMs was significantly higher compared with that in the controls ( $n=5$ ;  $P < 0.05$ ; Fig. 3D). Considering that there was a higher concentration of TGF- $\beta$  and IL-10 in the CAF-induced CAMs medium aforementioned, TGF- $\beta$ /Smad signaling might be activated only in the COC1 cells co-cultured with CAF-induced CAMs. These results demonstrated that the CAM-derived medium led to the activation of TGF- $\beta$ /Smad and increased the expression of EMT associated molecules.

*Significantly increased expression of IL-33 in CAFs and exosomes from CAFs compared with NOFs.* To verify that the extracellular vesicles could load and transport secretory proteins from CAFs to other cells, the exosomes were isolated and then the concentration of total proteins wrapped in these extracellular vesicles was measured. The shape and size of exosomes in the supernatant of NOFs and CAFs was assessed using transmission electron microscopy (Fig. 4A). The mean diameter and concentration per milliliter of exosomes were calculated and it was reported that the exosomes had a similar mean diameter between the supernatant of NOFs and CAFs and a significantly higher concentration in the exosomes isolated from CAFs compared with NOFs (Fig. 4B and C;  $P < 0.05$  and  $P < 0.01$  respectively). In addition, the amount of total protein in exosomes from CAFs was significantly higher compared with that in NOFs ( $n=5$ ,  $P < 0.05$ ; Fig. 4D). Next, we measured the expression of IL-33 in exosomes and cells. There was a significantly higher expression of IL-33 in exosomes from CAFs and CAMs compared with NOFs ( $n=5$ ; both  $P < 0.05$ ; Fig. 4E and F). These data demonstrated that the exosomes released by CAFs indeed act as a carrier of IL-33 and might deliver secretory proteins to other cells.

*Enhanced invasion and metastasis in ovarian cancer cells co-cultured with CAF-induced CAMs.* In order to verify the alteration in cancerous biological phenotypes, the invasion and migration of COC1 cells stimulated by CAF-derived medium and co-cultured with CAF-induced CAMs were measured using Transwell assays. As expected, there were no significant differences in the invasion and migration between COC1 cells stimulated with CAF-derived medium or not ( $n=5$ ;  $P > 0.05$ ; Fig. 5A). However, there were significant differences in the invasion and migration between COC1 cells co-cultured with CAF-induced CAMs or not ( $n=5$ ;  $P < 0.001$ ; Fig. 5B). In addition, the expression of apoptosis-related proteins, such as cleaved caspase-3 and -8, was detected in COC1 cells stimulated with CAF-derived medium and co-cultured with CAF-induced CAMs. No differences in the expression of apoptosis-related proteins were found in COC1 cells under either condition compared with the controls ( $n=5$ ;  $P > 0.05$ ; Fig. 5C and D). The chemotherapeutic resistance in COC1 cells under either condition compared with the controls ( $n=5$ ;  $P > 0.05$ ; Fig. 5C and D). The chemotherapeutic resistance in COC1 cells stimulated with CAF-derived medium and co-cultured with CAF-induced CAMs was also analyzed. Using MTT assays, similar cell viabilities of COC1 cells were reported after the administration of cisplatin at concentrations of 4, 8 and 16  $\mu\text{g/ml}$  in the COC1 cells stimulated with CAF-derived medium and controls ( $n=5$ ; Fig. 5E). Similar results were obtained for COC1 cells co-cultured with CAF-induced CAMs. A similar viability of COC1 cells was also found after administration of cisplatin at concentrations of 4, 8 and 16  $\mu\text{g/ml}$  in COC1 cells co-cultured with CAF-induced CAMs ( $n=5$ ; Fig. 5F).

*Mice with ST2-deficiency show a significantly reduced volume of xenografts after transplantation of human-derived primary ovarian cancer cells.* Xenograft transplantation was performed in NOD-SCID and NOD-SCID ST2-deficient mice. The expression of IL-33 in ST2 transplant tissues was also measured. It was

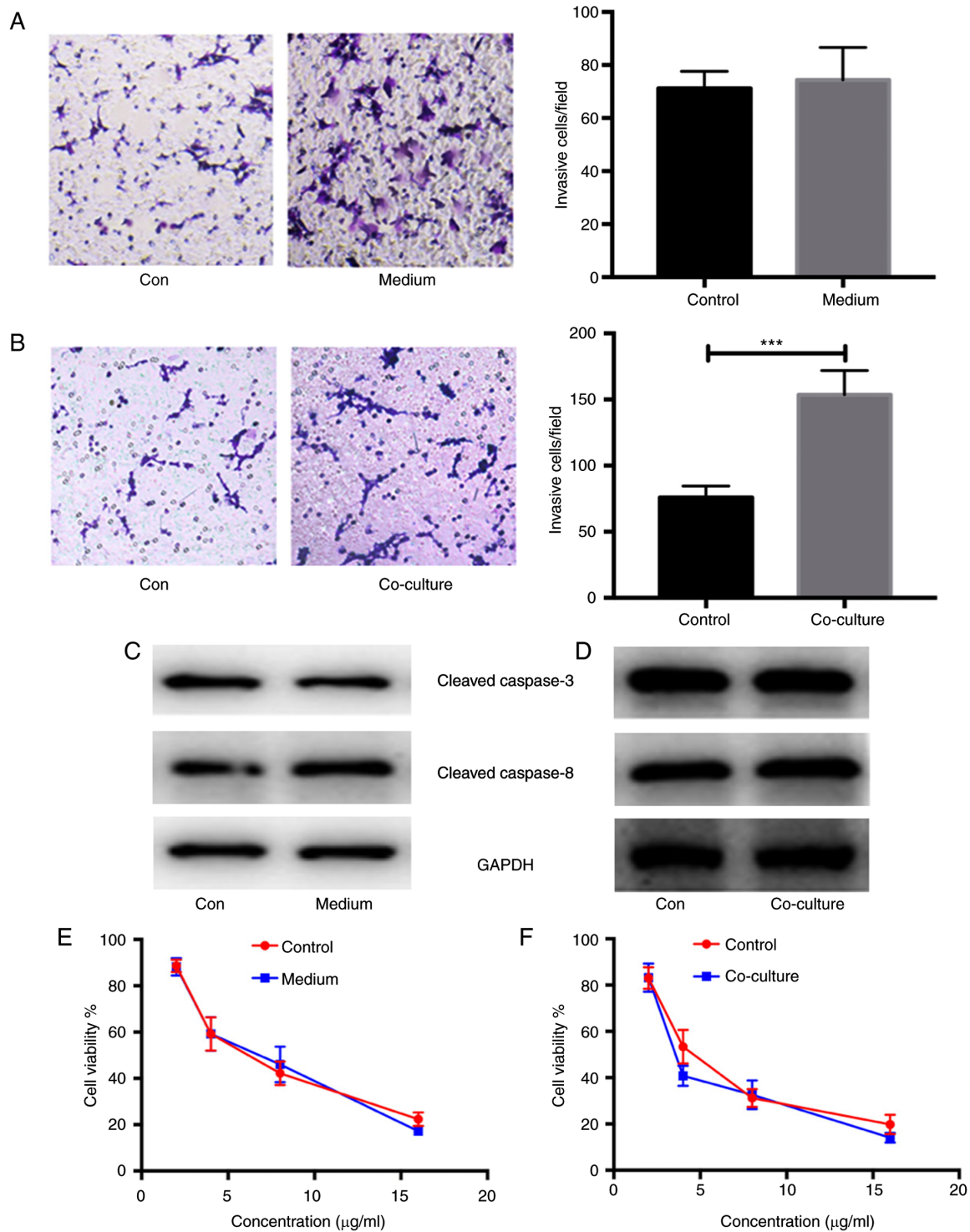


Figure 5. Enhanced invasion and migration in the ovarian cancerous cells in the ovarian cancerous cells co-cultured by CAF-induced CAMs. Invasion and migration of (A) COC1 cells stimulated by CAFs-derived medium or not and (B) COC1 cells co-cultured with CAF-induced CAMs or not. Expressions of apoptosis-related proteins (C) cleaved caspase-3 and caspase-8 in the COC1 cells stimulated by CAFs-derived medium and (D) co-cultured with CAF-induced CAMs. Chemotherapeutic resistance analysis about the COC1 cells stimulated with (E) CAFs-derived medium and (F) co-cultured with CAF-induced CAMs. The statistical analysis was performed by Student's t-test or one-way ANOVA analysis. \*\*\* $P < 0.001$ . Con, control; CAF, cancer-associated fibroblasts; CAM, cancer-associated macrophage.

demonstrated that the expression of IL-33 was similar between transplant tissues from WT and ST2-deficient mice ( $n=6$ ;  $P > 0.05$ ; Fig. 6A). However, the expression of ST2 in the xenograft tissues was almost undetectable from the NOD-SCID ST2-deficient mice and was significantly lower compared with that in NOD-SCID WT mice ( $n=6$ ;  $P < 0.01$ ; Fig. 6A). In addition, the expression of

EMT markers was significantly lower in ST2-deficient mice compared with that in WT mice ( $n=6$ ; Fig. 6B). The volume of xenografts from NOD-SCID ST2-deficient mice was significantly smaller compared with that of NOD-SCID WT mice ( $n=6$ ; both  $P < 0.05$ ; Fig. 6C and D). The data from *in vivo* experiments demonstrated that the blockade of IL-33/ST2 signaling

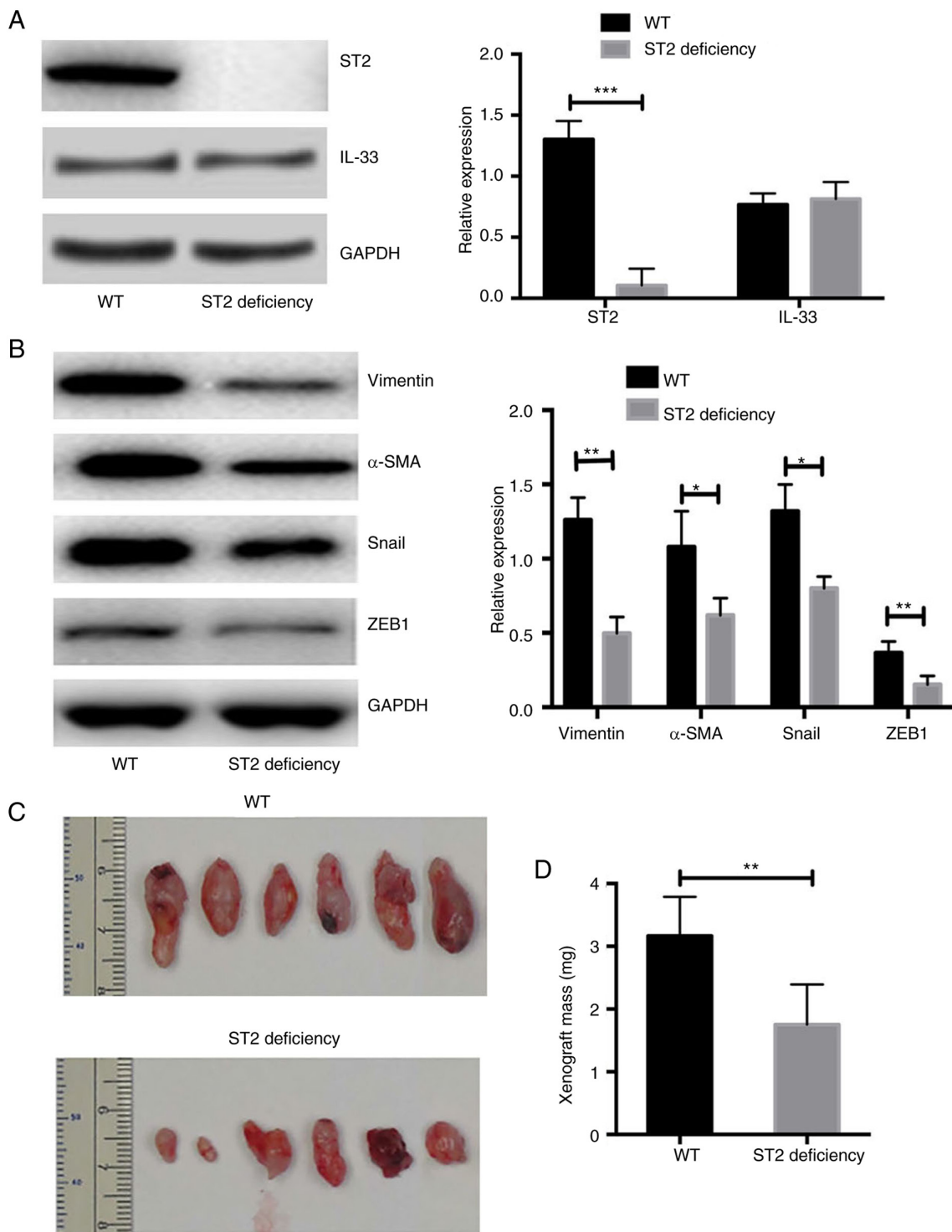


Figure 6. Mice with ST2-deficiency show a significantly reduced volume of xenograft after transplantation of human-derived primary ovarian cancer cells. Expressions of (A) IL-33 and (B) ST2 were similar between transplant tissues respectively from NOD-SCID WT and NOD-SCID ST2-deficiency mice. (C) Volume of xenograft after transplantation of human-derived primary ovarian cancer cells in the WT and ST2-deficiency mice. (D) Statistical analysis of tumor mass of xenograft after transplantation of human-derived primary ovarian cancer cells in the WT and ST2-deficiency mice. \* $P < 0.05$ , \*\* $P < 0.01$  and \*\*\* $P < 0.001$ . WT, wild-type; ST2, interleukin-1 receptor-like 1.

repressed the EMT process and reduced the volume of xenografts of human-derived primary ovarian cancer cells.

## Discussion

Interactions between cancer exosomes secreted from cancer-associated fibroblasts and the tumor microenvironment

have been brought into focus in recent years. There is evidence that the exosomes secreted from fibroblasts could impact the biological processes of cancer cells, induce immune repression and drive the formation of a disease-associated microenvironment (19,20). Although such data are lacking for ovarian cancer currently, studies have shown that exosomes derived from CAFs could regulate the function of immune cells in various cancer

types, such as breast cancer, pancreatic cancer and laryngeal squamous cell carcinoma (19-22). The main goal of the present study was to investigate the effect of exosomes isolated from cultured primary CAFs on blood-derived monocytes and their secondary influence on ovarian cancer cells.

The interplay between cancer-associated inflammatory cells and CAFs is complex, and some investigations have uncovered underlying mechanisms related to tumor invasion and metastasis (23-25). A previous study reported that primary human monocytes have a tendency to develop into immunosuppressive myeloid cells, characterized by the expression of the myeloid-derived suppressor cell marker S100A9, in a triple-negative (TN) breast cancer environment (25). This results in the activation of cancer-associated fibroblasts and the expression of CXCL16, which is a monocyte chemoattractant (26). This feedback loop promotes the formation of a reactive stroma, contributing to the aggressive and invasive phenotype of TN breast tumors (26). In colorectal cancer, molecular subgroups and microenvironmental signatures are highly correlated (26). In contrast to the good-prognosis microsatellite instability-enriched subgroup characterized by overexpression of genes specific to cytotoxic lymphocytes, the poor-prognosis mesenchymal subgroup (CMS4) expresses markers of lymphocytes and cells of monocytic origin. Pathological examination of CRC tissues also revealed that the mesenchymal subtype is characterized by a prominent infiltration of fibroblasts that likely produce chemokines and cytokines that favor tumor-associated inflammation and support angiogenesis, resulting in a poor prognosis (27).

Another study investigated the role of prostate CAFs in tumor biology. CAFs in prostate cancer could recruit monocytes into cancerous tissues and enhance their trans-differentiation toward the M2 macrophage phenotype. The study demonstrated that M2 macrophages and CAFs interact with each other, as M2 macrophages could promote the mesenchymal-mesenchymal transition of fibroblasts, leading to increased recruitment and the effects of M2 macrophage differentiation regulation on recruited monocytes. On the other hand, prostate cancer cells also participate in crosstalk through secretion of monocyte chemoattractant protein-1, facilitating monocyte recruitment and M2 polarization. Finally, this complicated crosstalk among cancer cells, CAFs and M2 macrophages leads to an enhancement of tumor cell motility, which promotes cancer cells metastasis from the primary tumor, as well as angiogenesis (28). The study illustrated that the interplay between CAFs and CAMs could influence the tumor biological phenotypes in prostate cancer by promoting the differentiation of M2 macrophages.

The present study demonstrated that IL-33 could play a role in migration and invasion in the progression of ovarian cancer as a secretion cytokine, which might be attributed to the interplay between CAFs and CAMs. CAMs exhibit an M2-like phenotype in the presence of IL-33 from secreted exosomes and ultimately alter the tumor microenvironment (28). Liu *et al* (29) revealed that IL-33 could have a direct tumor-promoting effect on COC1 cells, which could increase cell proliferation and inhibit apoptosis *in vitro*. IL-33 also predicts poor prognosis and promotes the proliferation of cancerous cells through the ERK and JNK signaling pathways. Previous studies have demonstrated the association between IL-33 and tumorigenesis, but

only the direct influence of IL-33/ST2 signaling on cancerous cells was investigated (30,31). The current study demonstrated that IL-33 could influence the tumor microenvironment and integrate the biological roles of CAMs and CAFs in the development of ovarian cancer.

The present study reported that exosomes from CAFs in ovarian cancer promoted M2 macrophage polarization, which led to enhanced EMT by TGF- $\beta$ /Smad signaling and a deteriorative invasive phenotype in cancerous cells. The indirect effect of CAFs on cancerous cells in ovarian cancer could be dependent on M2 macrophage polarization. It was demonstrated that exosomes derived from CAFs did not directly affect the biological phenotype of cancerous cells but could remodel the microenvironment by regulating immune cell function and differentiation. Therefore, CAFs and the interplay between CAFs and CAMs might be potential therapeutic targets in the inhibition of invasion and metastasis in ovarian cancer.

### Acknowledgements

The authors would like to thank Dr Jing Ren (Department of Biochemistry and Molecular Biology, Xi'an Medical College, Xi'an, Shaanxi, China) for help with the experimental design of the study.

### Funding

The study was supported by The National Natural Science Foundation of China (grant no. 81615924).

### Availability of data and materials

All data generated or analyzed during this study are included in this published article.

### Authors' contributions

CF and LK participated in the experimental design and data analysis. PY performed some of the experiments. YJ and CF conceived the project, performed most of the experiments and wrote the manuscript. CF and YJ confirm the authenticity of all the raw data. All the authors read and approved the final manuscript.

### Ethics approval and consent to participate

All procedures performed in studies involving human participants were in accordance with the ethical standards of the Baoji People's Hospital Ethics Committee and with the 1964 Helsinki declaration and its later amendments or comparable ethical standards. The protocols for animal experiments were approved by the Baoji People's Hospital Ethics Committee on the Use of Live Animals in Teaching and Research (Baoji, China) (approval no. 2018-129). Informed consent was obtained from all individual participants included in the study.

### Patient consent for publication

Not applicable.

## Competing interests

The authors declare that they have no competing interests.

## References

- Machida H, Matsuo K, Yamagami W, Ebina Y, Kobayashi Y, Tabata T, Kanauchi M, Nagase S, Enomoto T and Mikami M: Trends and characteristics of epithelial ovarian cancer in Japan between 2002 and 2015: A JSGO-JSOG joint study. *Gynecol Oncol* 153: 589-596, 2019.
- Rose PG, Java JJ, Salani R, Geller MA, Secord AA, Tewari KS, Bender DP, Mutch DG, Friedlander ML, Van Le L, *et al*: Nomogram for predicting individual survival after recurrence of advanced-stage, high-grade ovarian carcinoma. *Obstet Gynecol* 133: 245-254, 2019.
- Zhang J, Silva EG, Sood AK, *et al*: Ovarian epithelial carcinogenesis[M]//gynecologic and obstetric pathology, Volume 2. Springer, Singapore, pp121-139, 2019.
- Hwang JY, Lim WY, Tan CS, Lim SL, Chia J, Chow KY and Chay WY: Ovarian cancer incidence in the multi-ethnic asian city-state of Singapore 1968-2012. *Asian Pac J Cancer Prev* 20: 3563-3569, 2019.
- Sahai E, Astsaturon I, Cukierman E, DeNardo DG, Egeblad M, Evans RM, Fearon D, Greten FR, Hingorani SR, Hunter T, *et al*: A framework for advancing our understanding of cancer-associated fibroblasts. *Nat Rev Cancer* 20: 174-186, 2020.
- Tsang M, Quesnel K, Vincent K, Hutchenreuther J, Postovit LM and Leask A: Insights into fibroblast plasticity: Cellular communication network 2 is required for activation of cancer-associated fibroblasts in a murine model of melanoma. *Am J Pathol* 190: 206-221, 2020.
- Ling J and Chiao PJ: Two birds with one stone: Therapeutic targeting of IL-1 $\beta$  signaling pathways in pancreatic ductal adenocarcinoma and the cancer-associated fibroblasts. *Cancer Discov* 9: 173-175, 2019.
- Neri S, Hashimoto H, Kii H, Watanabe H, Masutomi K, Kuwata T, Date H, Tsuboi M, Goto K, Ochiai A and Ishii G: Cancer cell invasion driven by extracellular matrix remodeling is dependent on the properties of cancer-associated fibroblasts. *J Cancer Res Clin Oncol* 142: 437-446, 2016.
- Teng F, Tian WY, Wang YM, Zhang YF, Guo F, Zhao J, Gao C and Xue FX: Cancer-associated fibroblasts promote the progression of endometrial cancer via the SDF-1/CXCR4 axis. *J Hematol Oncol* 9: 8, 2016.
- Ogawa K, Lin Q, Li L, Bai X, Chen X, Chen H, Kong R, Wang Y, Zhu H, He F, *et al*: Prometastatic secretome trafficking via exosomes initiates pancreatic cancer pulmonary metastasis. *Cancer Lett* 481: 63-75, 2020.
- Arai K, Ishimatsu H, Iwasaki T, Tsuchiya C, Sonoda A and Ohata K: Membranous S100A10 involvement in the tumor budding of colorectal cancer during oncogenesis: Report of two cases with immunohistochemical analysis. *World J Surg Oncol* 18: 289, 2020.
- Brunetto E, De Monte L, Balzano G, Camisa B, Laino V, Riba M, Heltai S, Bianchi M, Bordignon C, Falconi M, *et al*: The IL-1/IL-1 receptor axis and tumor cell released inflammasome adaptor ASC are key regulators of TSLP secretion by cancer associated fibroblasts in pancreatic cancer. *J Immunother Cancer* 7: 45, 2019.
- Kobayashi H, Enomoto A, Woods SL, Burt AD, Takahashi M and Worthley DL: Cancer-associated fibroblasts in gastrointestinal cancer. *Nat Rev Gastroenterol Hepatol* 16: 282-295, 2019.
- Qian L, Tang Z, Yin S, Mo F, Yang X, Hou X, Liu A and Lu X: Fusion of dendritic cells and cancer-associated fibroblasts for activation of anti-tumor cytotoxic T lymphocytes. *J Biomed Nanotechnol* 14: 1826-1835, 2018.
- Suklabaidya S, Dash P and Senapati S: Pancreatic fibroblast exosomes regulate survival of cancer cells. *Oncogene* 36: 3648-3649, 2017.
- Kanada M, Bachmann MH and Contag CH: Signaling by extracellular vesicles advances cancer hallmarks. *Trends Cancer* 2: 84-94, 2016.
- Yang F, Ning Z, Ma L, Liu W, Shao C, Shu Y and Shen H: Exosomal miRNAs and miRNA dysregulation in cancer-associated fibroblasts. *Mol Cancer* 16: 148, 2017.
- Ringuette Goulet C, Bernard G, Tremblay S, Chabaud S, Bolduc S and Pouliot F: Exosomes induce fibroblast differentiation into Cancer-associated fibroblasts through TGF- $\beta$  signaling. *Mol Cancer Res* 16: 1196-1204, 2018.
- Wang H, Wei H, Wang J, Li L, Chen A and Li Z: MicroRNA-181d-5p-containing exosomes derived from CAFs promote EMT by regulating CDX2/HOXA5 in breast cancer. *Mol Ther Nucleic Acids* 19: 654-667, 2020.
- Yeon JH, Jeong HE, Seo H, Cho S, Kim K, Na D, Chung S, Park J, Choi N and Kang JY: Cancer-derived exosomes trigger endothelial to mesenchymal transition followed by the induction of cancer-associated fibroblasts. *Acta Biomater* 76: 146-153, 2018.
- Qin X, Guo H, Wang X, Zhu X, Yan M, Wang X, Xu Q, Shi J, Lu E, Chen W and Zhang J: Exosomal miR-196a derived from cancer-associated fibroblasts confers cisplatin resistance in head and neck cancer through targeting CDKN1B and ING5. *Genome Biol* 20: 12-14, 2019.
- Li K, Chen Y, Li A, Tan C and Liu X: Exosomes play roles in sequential processes of tumor metastasis. *Int J Cancer* 144: 1486-1495, 2019.
- Liu T and Kong J: CAF-derived exosomes remodel ECM by targeting lung fibroblasts via integrin  $\alpha\beta$ 1 at the pre-metastatic niche. *J Extracellular Vesicles* 7: 234-235, 2018.
- Guo H, Ha C, Dong H, Yang Z, Ma Y and Ding Y: Cancer-associated fibroblast-derived exosomal microRNA-98-5p promotes cisplatin resistance in ovarian cancer by targeting CDKN1A. *Cancer Cell Int* 19: 347, 2019.
- Wu HJ, Hao M, Yeo SK and Guan JL: FAK signaling in cancer-associated fibroblasts promotes breast cancer cell migration and metastasis by exosomal miRNAs-mediated intercellular communication. *Oncogene* 39: 2539-2549, 2020.
- Allaoui R, Bergenfelz C, Mohlin S, Hagerling C, Salari K, Werb Z, Anderson RL, Ethier SP, Jirström K, Pählman S, *et al*: Cancer-associated fibroblast-secreted CXCL16 attracts monocytes to promote stroma activation in triple-negative breast cancers. *Nat Commun* 7: 13050, 2016.
- Becht E, de Reyniès A, Giraldo NA, Pilati C, Buttard B, Lacroix L, Selves J, Sautès-Fridman C, Laurent-Puig P and Fridman WH: Immune and stromal classification of colorectal cancer is associated with molecular subtypes and relevant for precision immunotherapy. *Clin Cancer Res* 22: 4057-4066, 2016.
- Comito G, Giannoni E, Segura CP, Barcellos-de-Souza P, Raspollini MR, Baroni G, Lanciotti M, Serni S and Chiarugi P: Cancer-associated fibroblasts and M2-polarized macrophages synergize during prostate carcinoma progression. *Oncogene* 33: 2423-2431, 2014.
- Liu X, Hansen DM, Timko NJ, Zhu Z, Ames A, Qin C, Nicholl MB, Bai Q, Chen X, Wakefield MR, *et al*: Association between interleukin-33 and ovarian cancer. *Oncol Rep* 41: 1045-1050, 2019.
- Tong X, Barbour M, Hou K, Gao C, Cao S, Zheng J, Zhao Y, Mu R and Jiang HR: Interleukin-33 predicts poor prognosis and promotes ovarian cancer cell growth and metastasis through regulating ERK and JNK signaling pathways. *Mol Oncol* 10: 113-125, 2016.
- Larsen KM, Minaya MK, Vaish V and Peña MMO: The role of IL-33/ST2 pathway in tumorigenesis. *Int J Mol Sci* 19: 2676, 2018.



This work is licensed under a Creative Commons Attribution-NonCommercial-NoDerivatives 4.0 International (CC BY-NC-ND 4.0) License.